INL REPORT

INL/EXT-19-54395
Unlimited Release
Printed March 2020

Sockeye Theory Manual

J. E. Hansel, R. A. Berry, D. Andrs, R. C. Martineau

Prepared by
Idaho National Laboratory
Idaho Falls, Idaho 83415

The Idaho National Laboratory is a multiprogram laboratory operated by
Battelle Energy Alliance for the United States Department of Energy
under DOE Idaho Operations Office. Contract DE-AC07-05ID14517.

Issued by the Idaho National Laboratory, operated for the United States Department of Energy by Battelle Energy Alliance.

INL/EXT-19-54395
Unlimited Release
Printed March 2020

Sockeye Theory Manual

J. E. Hansel, R. A. Berry, D. Andrs, R. C. Martineau

Contents

Appendix

Figures

Tables

1 Introduction

Sockeye is an application that models heat pipe performance, based on the MOOSE framework[1]. Its primary focus is on liquid-metal heat pipes with annular screen or porous wick structures, with the intended application being the simulation of heat pipes in microreactors. The purpose of this capability is to evaluate and understand heat pipe performance under different conditions. Furthermore, this heat pipe performance is intended to be coupled to multiphysics applications for modeling microreactors, so that the effects of heat pipe performance on the larger reactor system can be simulated.

1.1 Types of Heat Pipes Modeled

Sockeye is developed for the purpose of modeling heat pipes for use in microreactors. The heat pipes considered for this application is of the "conventional" type, where a sealed cylindrical tube contains a wick structure along the inner surface, which is saturated with a liquid. This wick structure may or may not be flush against the inner wall of the tube; if not, there can be a thin annular channel along which liquid may flow, in addition to through the wick structure. Though the wick and liquid channels are annular, this design is not to be confused with "annular" heat pipes, in which the container is not a sealed cylinder but a sealed annular tube; in that design, heat transfer occurs through both the outer and inner walls[2].

Wick structures are assumed to be of an annular, homogeneous design, such as wrapped wire screens, sintered metal, or open annulus screen. Arterial designs, for example, are not currently planned for consideration.

Working fluids considered are those suitable for the high operating temperatures encountered in a microreactor design; e.g., sodium, potassium, and NaK. However, currently models do not prevent the modeling of lower-temperature working fluids such as water.

1.2 Current Capabilities

Sockeye can model the two-phase flow of the working fluid inside the heat pipe container, using a 1-D approximation, under normal operation, i.e., with the working fluid fully melted and with the vapor and liquid phases occupying the core and wick/annulus

regions, respectively. Thus, accident scenarios such as dryout are not yet capable of being simulated. The flow solution provides the thermodynamic state of each phase, the axial velocities of each phase, and the volume fractions of the phases. See Section 3.

Sockeye provides the capability for modeling heat conduction in 2-D, through the heat pipe walls (and any other structure exterior to the working fluid flow). Boundary conditions on this heat conduction domain can be linked to the 1-D flow channel, to externally imposed boundary conditions such as a specified heat flux or surface temperature, or to an external application providing temperature or heat flux.

For startup, Sockeye currently can perform aggregate heat transfer to the frozen working fluid until certain conditions are met, at which point the two-phase flow simulation can begin. See Section 4.1.

Lastly, Sockeye has the ability to coupled to other MOOSE-based applications. The primary mode of coupling will be through heat transfer boundary conditions between the applications, specified from either heat flux or temperatures of each side. See Section 5.

1.3 Planned Future Capabilities

Currently, Sockeye assumes a flow configuration that does not include accident scenarios such as dryout, but future plans include this two-phase flow capability.

Sockeye is planned to model both startup and shutdown transients, most likely with a 1-D model that incorporates 3-phase flow. This may add, for example, a volume fraction corresponding to the solid phase and some interfacial terms between the solid phase and other two phases.

Sockeye is planned to predict various operating limits of heat pipe operation and perhaps incorporate some of these into the simulation by forcibly limiting heat fluxes. See Section 2.

2 Operating Limits

A number of phenomena can limit the ability of a heat pipe to remove heat. Some of the main limits of interest are summarized in the sections that follow.

2.1 Capillary Limit

The capillary limit is derived by comparing the sum of the pressure drops around the heat pipe to the maximum pressure difference $\Delta p_{\text{cap,max}}$ that can be supported at the liquid-vapor interface:

$$\Delta p_{\text{evap}} + \Delta p_v + \Delta p_{\text{cond}} + \Delta p_{\ell,\text{flow}} + \Delta p_{\ell,g} \leq \Delta p_{\text{cap,max}} \,, \tag{1}$$

where

- $\Delta p_{\text{cap,max}}$ is the maximum pressure difference that can be supported at the liquid-vapor interface,
- Δp_{evap} is the pressure drop due to evaporation,
- Δp_{cond} is the pressure drop due to condensation,
- Δp_v is the pressure drop on the vapor side due to acceleration, friction, etc.,
- $\Delta p_{\ell,\text{flow}}$ is the pressure drop on the liquid side due to friction and porous drag, and
- $\Delta p_{\ell,g}$ is the pressure drop on the liquid side due to gravity (note this is negligible for the vapor side).

The maximum capillary pressure is given by

$$\Delta p_{\text{cap,max}} = \frac{2\sigma}{R_{\text{eff}}} \,, \tag{2}$$

where R_{eff} is the *effective pore radius*, which is ideally determined experimentally, but can be estimated analytically if needed.

Neglecting Δp_{evap}, Δp_{cond}, and Δp_v gives

$$\Delta p_{\ell,\text{flow}} + \Delta p_{\ell,g} \leq \Delta p_{\text{cap,max}} \,. \tag{3}$$

The gravity pressure drop is computed as

$$\Delta p_{\ell,g} = \rho_\ell g L_{\text{hp}} \sin\theta \,, \tag{4}$$

where

- L_{hp} is the total length of the heat pipe, and
- θ is the angle between the heat pipe and the horizontal at the condenser end (thus, $\theta = 0$ corresponds to horizontal, $\theta = -\frac{\pi}{2}$ corresponds to gravity-assisted, and $\theta = \frac{\pi}{2}$ corresponds to gravity-adverse).

Using Darcy's law, the liquid flow pressure drop is as follows:

$$\Delta p_{\ell,\text{flow}} = \frac{\mu_\ell L_{\text{eff}} \dot{m}}{\rho_\ell K A_\ell} \,, \tag{5}$$

where

- $L_{\text{eff}} = \frac{1}{2} L_{\text{evap}} + L_{\text{adia}} + \frac{1}{2} L_{\text{cond}}$ is the *effective length*,
- $\dot{m}$ is the mass flow rate,
- K is the permeability of the liquid channel, and
- A_ℓ is the cross-sectional area of the liquid channel.

Using $\dot{Q} = \dot{m} h_{\text{lat}}$ (where h_{lat} is the latent heat), the capillary limit is obtained [2, 3]:

$$\dot{Q} \leq \dot{Q}_{\text{max,cap}} \,, \tag{6}$$

$$\dot{Q}_{\text{max,cap}} = \frac{\rho_\ell \sigma h_{\text{lat}}}{\mu_\ell} \frac{K A_\ell}{L_{\text{eff}}} \left(\frac{2}{R_{\text{eff}}} - \frac{\rho_\ell g L_{\text{hp}}}{\sigma} \sin\theta \right) \,. \tag{7}$$

Figure 1 shows an example of the capillary limit for different inclinations.

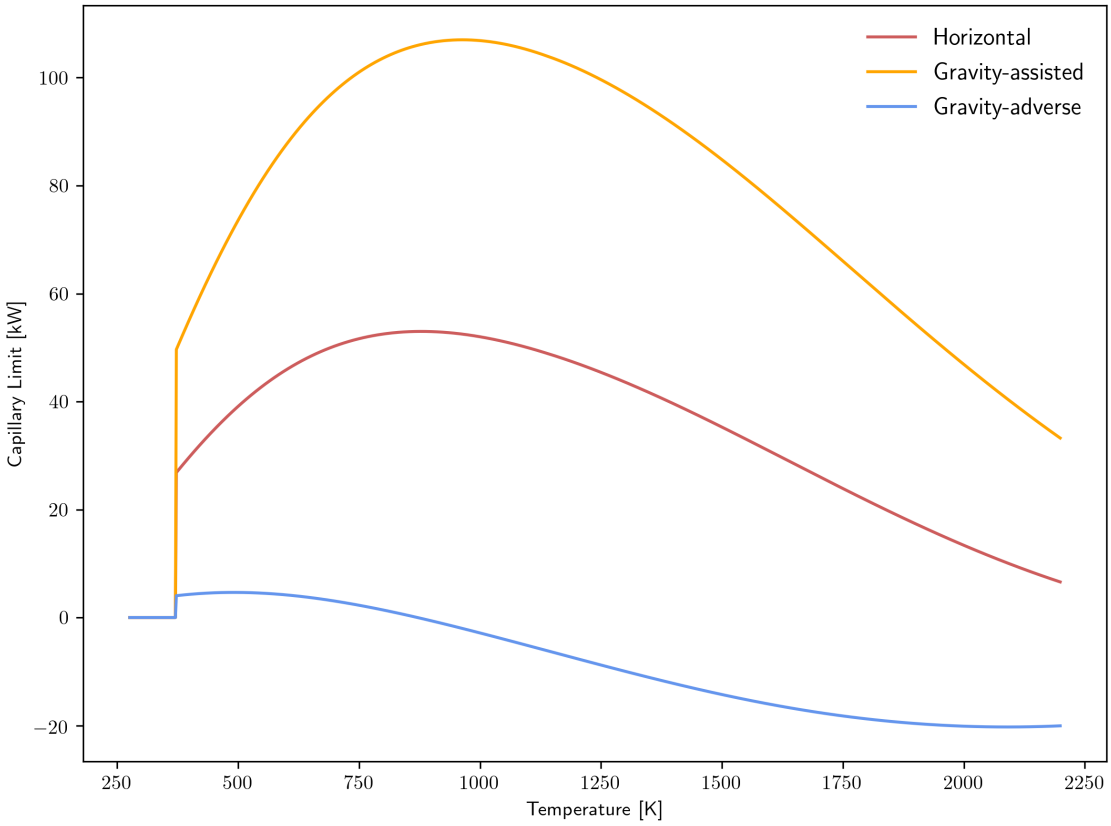

Figure 1: Capillary limits example for different heat pipe orientations

2.2 Entrainment Limit

The entrainment limit exists because the vapor phase can shear off liquid into the core vapor channel, thus reducing the rate at which liquid can return to the evaporator. Entrainment occurs when the shear force of the vapor overcomes the surface tension force. The Weber number is a dimensionless number that is a ratio of these two forces, and entrainment occurs when this number is greater than unity, thus leading to the following heat transfer rate limit [2]:

$$\dot{Q}_{\text{max,ent}} = A_v h_{\text{lat}} \left(\frac{\sigma \rho_v}{D_{h,\text{pore}}} \right)^{1/2} , \tag{8}$$

where

- $A_v = \frac{\pi D_v^2}{4}$ is the cross-sectional area of the vapor channel, and
- $D_{h,\text{pore}}$ is the hydraulic diameter of a pore.

2.3 Boiling Limit

The boiling limit occurs because bubble formation and departure can inhibit the ability of the liquid to return to the evaporator. This limit is estimated as follows [2]:

$$\dot{Q}_{\text{max,boil}} = \frac{4\pi L_{\text{evap}} k_{\text{eff}} \sigma T_v}{h_{\text{lat}} \rho_v \ln(D_{\text{hp,i}}/D_v)} \left(\frac{1}{R_b} - \frac{1}{R_{\text{men}}} \right) , \tag{9}$$

where

- k_{eff} is the effective thermal conductivity of the wick, which in general depends on the geometry and thermal conductivity of the wick structure itself, as well as the thermal conductivity of the liquid,
- $D_{\text{hp,i}}$ is the inner heat pipe wall diameter,
- D_v is the vapor channel diameter,
- R_b is the bubble radius ([2] notes that this could be taken to be 10^{-7} m for conventional heat pipes), and
- R_{men} is the meniscus radius at the liquid-vapor interface in the evaporator region ([2] notes that this could be estimated as being equal to R_{eff}).

2.4 Viscous Limit

The viscous limit occurs because the vapor pressure at the condenser end cap cannot be less than zero. By performing some analyses in the viscous flow regime, the following expression is obtained for the maximum heat transfer rate due to the viscous limit [2]:

$$\dot{Q}_{\text{max,vis}} = \frac{A_v^2 h_{\text{lat}} \rho_v p_v}{16\pi\mu_v L_{\text{eff}}}\,, \tag{10}$$

where

- $A_v = \frac{\pi D_v^2}{4}$ is the cross-sectional area of the vapor channel,
- ρ_v and p_v correspond to the vapor density and pressure, respectively, at the evaporator end cap, and
- $L_{\text{eff}} = \frac{1}{2}L_{\text{evap}} + L_{\text{adia}} + \frac{1}{2}L_{\text{cond}}$ is the effective length.

2.5 Sonic Limit

The sonic limit occurs because the flow becomes choked when it becomes sonic. An estimate for this limit is as follows [2]:

$$\dot{Q}_{\text{max,son}} = \frac{\rho_v c_v h_{\text{lat}} A_v}{(2(\gamma_v + 1))^{1/2}}\,, \tag{11}$$

where

- ρ_v, c_v, and γ_v are the vapor density, sound speed, and ratio of specific heats (c_p/c_v), respectively, all evaluated at the evaporator end cap, and
- $A_v = \frac{\pi D_v^2}{4}$ is the cross-sectional area of the vapor channel.

3 Two-Phase Flow Model

The two-phase flow model used in Sockeye adapts the two-phase flow model from RELAP-7[4], with the following changes:

- Wall mass transfer is turned off,
- Wall heat flux goes completely into the liquid phase,
- Heat conduction is added for the liquid phase,
- Interfacial velocity is assumed to be zero,
- Velocity relaxation is turned off, and
- Pressure relaxation is changed to account for capillary pressure: instead of relaxing toward $p_v = p_\ell$, pressures relax toward $p_v = p_\ell + \Delta p^{\text{cap}}_{\ell \to v}$, where $\Delta p^{\text{cap}}_{\ell \to v}$ is the capillary pressure difference.

With these modifications, the system of partial differential equations becomes the following:

$$\frac{\partial \alpha_\ell A}{\partial t} = \mu \left(p_\ell + \Delta p^{\text{cap}}_{\ell \to v} - p_v \right) A - \frac{\Gamma^{\text{int}}_{\ell \to v} a_{\text{int}} A}{\rho_{\text{int}}} \,, \tag{12}$$

$$\frac{\partial \alpha_\ell \rho_\ell A}{\partial t} + \frac{\partial \alpha_\ell \rho_\ell u_\ell A}{\partial x} = -\Gamma^{\text{int}}_{\ell \to v} a_{\text{int}} A \,, \tag{13}$$

$$\frac{\partial \alpha_\ell \rho_\ell u_\ell A}{\partial t} + \frac{\partial \alpha_\ell \left(\rho_\ell u_\ell^2 + p_\ell \right) A}{\partial x} = p_{\text{int}} \frac{\partial \alpha_\ell}{\partial x} A - F^{\text{wall}}_\ell A + \alpha_\ell \rho_\ell g_x A \,, \tag{14}$$

$$\begin{aligned} \frac{\partial \alpha_\ell \rho_\ell E_\ell A}{\partial t} + \frac{\partial \alpha_\ell u_\ell \left(\rho_\ell E_\ell + p_\ell \right) A}{\partial x} &= \frac{\partial}{\partial x} \left(\alpha_\ell k_\ell \frac{\partial T_\ell}{\partial x} A \right) \\ &\quad - \bar{p}_{\text{int}} \mu \left(p_\ell + \Delta p^{\text{cap}}_{\ell \to v} - p_v \right) A - F^{\text{wall}}_\ell u_\ell A + \alpha_\ell \rho_\ell g_x u_\ell A \\ &\quad + q_{\text{wall} \to \ell} P_{\text{wall}} + q_{\text{int} \to \ell} a_{\text{int}} A - \Gamma^{\text{int}}_{\ell \to v} E^{\text{int}}_\ell a_{\text{int}} A \,. \end{aligned} \tag{15}$$

$$\frac{\partial \alpha_v \rho_v A}{\partial t} + \frac{\partial \alpha_v \rho_v u_v A}{\partial x} = \Gamma^{\text{int}}_{\ell \to v} a_{\text{int}} A \,, \tag{16}$$

$$\frac{\partial \alpha_v \rho_v u_v A}{\partial t} + \frac{\partial \alpha_v \left(\rho_v u_v^2 + p_v\right) A}{\partial x} = p_{\text{int}} \frac{\partial \alpha_v}{\partial x} A - F_v^{\text{wall}} A + \alpha_v \rho_v g_x A \,, \tag{17}$$

$$\begin{aligned} \frac{\partial \alpha_v \rho_v E_v A}{\partial t} + \frac{\partial \alpha_v u_v \left(\rho_v E_v + p_v\right) A}{\partial x} \\ = \bar{p}_{\text{int}} \mu \left(p_\ell + \Delta p_{\ell \to v}^{\text{cap}} - p_v\right) A - F_v^{\text{wall}} u_v A + \alpha_v \rho_v g_x u_v A \\ + q_{\text{wall} \to v} P_{\text{wall}} + q_{\text{int} \to v} a_{\text{int}} A + \Gamma_{\ell \to v}^{\text{int}} E_v^{\text{int}} a_{\text{int}} A \,. \end{aligned} \tag{18}$$

Note that the volume fraction equation is needed for only one of the phases due to the relation $\alpha_\ell + \alpha_v = 1$.

Interfacial variable expressions are derived from local Riemann problem solutions [5][6]:

$$\bar{p}_{\text{int}} \equiv \frac{Z_\ell p_v + Z_v p_\ell}{Z_\ell + Z_v} \,, \tag{19}$$

$$p_{\text{int}} \equiv \bar{p}_{\text{int}} + \frac{Z_\ell Z_v}{Z_\ell + Z_v} \text{sgn} \frac{\partial \alpha_\ell}{\partial x} (u_v - u_\ell) \,, \tag{20}$$

$$\rho_{\text{int}} \equiv \rho_\ell (T_{\text{int}}, \bar{p}_{\text{int}}) \,, \tag{21}$$

$$h_k^{\text{int}} \equiv h_k (\bar{p}_{\text{int}}, T_{\text{int}}) \,, \tag{22}$$

$$H_k^{\text{int}} \equiv h_k^{\text{int}} + \frac{1}{2} u_{\text{int}}^2 \,, \tag{23}$$

$$E_k^{\text{int}} \equiv H_k^{\text{int}} - \frac{p_{\text{int}}}{\rho_{\text{int}}} \,. \tag{24}$$

$$T_{\text{int}} \equiv T_{\text{sat}} (\bar{p}_{\text{int}}) \,, \tag{25}$$

where Z_k is the acoustic impedance of phase k:

$$Z_k \equiv \rho_k c_k \,. \tag{26}$$

The pressure relaxation coefficient is defined as follows [5][6]:

$$\mu \equiv \frac{a_{\text{int}}}{Z_\ell + Z_v} \,. \tag{27}$$

3.1 Geometrical Parameters

Table 1 gives user-specified parameters, and Table 2 gives derived quantities. Note that A is shorthand for A_{flow}.

Table 1: User-provided geometrical parameters

Symbol	Description	Units
$D_{\text{hp,i}}$	Inner diameter of heat pipe	m
L_{hp}	Length of heat pipe	m
$D_{\text{wick,i}}$	Inner diameter of wick	m
$D_{\text{wick,o}}$	Outer diameter of wick	m
R_{pore}	Radius of a wick pore	m
ϵ	Porosity of wick	-

Table 2: Geometrical parameters

Symbol	Description	Units	Relation
$R_{\text{hp,i}}$	Inner radius of heat pipe	m	$R_{\text{hp,i}} = \frac{D_{\text{hp,i}}}{2}$
$R_{\text{wick,i}}$	Inner radius of wick	m	$R_{\text{wick,i}} = \frac{D_{\text{wick,i}}}{2}$
$R_{\text{wick,o}}$	Outer radius of wick	m	$R_{\text{wick,o}} = \frac{D_{\text{wick,o}}}{2}$
A_{hp}	Cross-sectional area of heat pipe	m^2	$A_{\text{hp}} = \pi R_{\text{hp}}^2$
A_{core}	Cross-sectional area of core region	m^2	$A_{\text{core}} = \pi R_{\text{wick,i}}^2$
A_{wick}	Cross-sectional area of wick region	m^2	$A_{\text{wick}} = \pi(R_{\text{wick,o}}^2 - R_{\text{wick,i}}^2)$
A_{ann}	Cross-sectional area of annulus region	m^2	$A_{\text{ann}} = A_{\text{hp}} - A_{\text{core}} - A_{\text{wick}}$
A_{flow}	Cross-sectional flow area	m^2	$A_{\text{flow}} = A_{\text{core}} + \epsilon A_{\text{wick}} + A_{\text{ann}}$
A_{pore}	Cross-sectional area of a wick pore	m^2	$A_{\text{pore}} = \pi R_{\text{pore}}^2$
V_{flow}	Total flow volume	m^3	$V_{\text{flow}} = A_{\text{flow}} L_{\text{hp}}$
$V_{\text{pore,hemi}}$	Hemispherical pore volume	m^3	$V_{\text{pore,hemi}} = \frac{2}{3}\pi R_{\text{pore}}^3$

The assumed heat pipe cross section is illustrated in Figure 2, which illustrates the radial dimensions of the heat pipe. For this heat pipe configuration, during normal operation, the liquid phase resides in the outer (annular) region, and the vapor phase resides in the center (core) region.

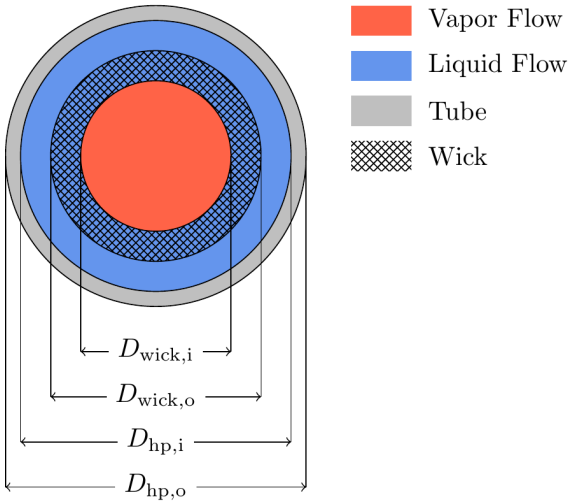

Figure 2: Cross section of a heat pipe modeled with Sockeye

To compute quantities such as the capillary pressure $\Delta p^{\text{cap}}_{\ell \to v}$ and the interfacial area density a_{int}, a 2-phase flow topology is determined from the void fraction and geometrical quantities. Table 3 lists these flow regimes, and Table 4 defines the associated bounding void fraction values, which are computed as follows:

$$\alpha_v^{\text{wick,i,0}} = \frac{A_{\text{core}}}{A_{\text{flow}}}\,, \tag{28a}$$

$$\alpha_v^{\text{wick,i,}-} = \alpha_v^{\text{wick,i,0}} - N'''_{\text{pore}}(D_{\text{wick,i}})V_{\text{pore,hemi}}\,, \tag{28b}$$

$$\alpha_v^{\text{wick,i,}+} = \alpha_v^{\text{wick,i,0}} + N'''_{\text{pore}}(D_{\text{wick,i}})V_{\text{pore,hemi}}\,, \tag{28c}$$

$$\alpha_v^{\text{wick,o,}+} = \frac{A_{\text{core}} + \epsilon A_{\text{wick}}}{A_{\text{flow}}} + N'''_{\text{pore}}(D_{\text{wick,o}})V_{\text{pore,hemi}}\,. \tag{28d}$$

The pore density $N'''_{\text{pore}}(D)$ is computed as follows. First, the number of pores on a wick surface needs to be estimated. For some diameter D within the wick ($D_{\text{wick,i}} \leq D \leq D_{\text{wick,o}}$), the corresponding surface area is $\pi D L_{\text{hp}}$, and using the user-provided provided porosity, the total area of pores on that surface is $\epsilon \pi D L_{\text{hp}}$. Dividing this by the cross-sectional area per pore then gives the number of pores N_{pore} on the surface:

$$N_{\text{pore}}(D) = \frac{\epsilon \pi D L_{\text{hp}}}{A_{\text{pore}}}\,. \tag{29}$$

The number of pores per unit flow volume is then

$$N'''_{\text{pore}}(D) = \frac{N_{\text{pore}}(D)}{L_{\text{hp}} A_{\text{flow}}} = \frac{\epsilon \pi D}{A_{\text{pore}} A_{\text{flow}}} \,. \tag{30}$$

Table 3: Interface location cases

Case	Description
$\alpha_v \leq \alpha_v^{\text{wick,i,}-}$	Flat, inside the inner surface of the wick
$\alpha_v^{\text{wick,i,}-} < \alpha_v \leq \alpha_v^{\text{wick,i,}+}$	Curved or flat, about the inner surface of the wick
$\alpha_v^{\text{wick,i,}+} < \alpha_v \leq \alpha_v^{\text{wick,o,}+}$	Curved outward into the annulus from the wick, outside the inner surface of the wick and inside or at the outer surface of the wick
$\alpha_v > \alpha_v^{\text{wick,o,}+}$	Flat, outside the outer surface of the wick

Table 4: Void fraction bound quantities

Symbol	Description
$\alpha_v^{\text{wick,i,}-}$	Inner wick surface, hemispherical volumes inward
$\alpha_v^{\text{wick,i,0}}$	Inner wick surface, flat interface
$\alpha_v^{\text{wick,i,}+}$	Inner wick surface, hemispherical volumes outward
$\alpha_v^{\text{wick,o,}+}$	Outer wick surface, hemispherical volumes outward

3.2 Closures

3.2.1 Contact Angle

The capillary pressure difference between the phases and the interfacial area density both depend on the curvature of the liquid-vapor interface. The contact angle θ_{cap} of this interface is defined such that

$$\cos \theta_{\text{cap}} = \frac{R_{\text{pore}}}{R_{\text{cap}}} \,, \tag{31}$$

where R_{cap} is the capillary radius, or radius of curvature, of the interface. Figure 3 gives an illustration of the contact angle.

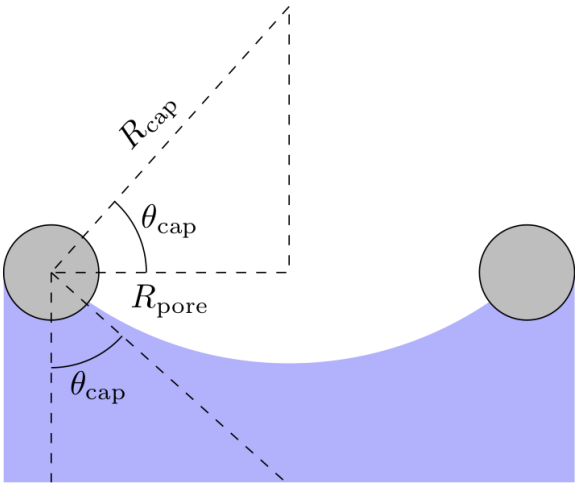

Figure 3: Contact angle definition

Let ξ denote the sine of the contact angle:

$$\xi \equiv \sin\theta_{\text{cap}} \,. \tag{32}$$

Combining these two relations gives

$$R_{\text{cap}}(\xi) = \frac{R_{\text{pore}}}{\cos\theta_{\text{cap}}} = \frac{R_{\text{pore}}}{\sqrt{1-\xi^2}} \,. \tag{33}$$

As suggested by Table 3, for the cases $\alpha_v \leq \alpha_v^{\text{wick,i,}-}$ and $\alpha_v > \alpha_v^{\text{wick,o,}+}$, the interface is flat:

$$\xi = 1 \,, \qquad \alpha_v \leq \alpha_v^{\text{wick,i,}-} \quad \text{or} \quad \alpha_v > \alpha_v^{\text{wick,o,}+} \,. \tag{34}$$

For the case $\alpha_v^{\text{wick,i,}+} < \alpha_v \leq \alpha_v^{\text{wick,o,}+}$, the interface is fully curved outward with the radius of the pore. Thus,

$$\xi = 0 \,, \qquad \alpha_v^{\text{wick,i,}+} < \alpha_v \leq \alpha_v^{\text{wick,o,}+} \,. \tag{35}$$

Finally, for the case $\alpha_v^{\text{wick,i,}-} < \alpha_v \leq \alpha_v^{\text{wick,o,}+}$, the interface has a radius of curvature between R_{pore} (fully curved) and infinity (flat). In this region, the void fraction can be related to ξ as follows:

$$\alpha_v(\xi) = \begin{cases} \alpha_v^{\text{wick,i,0}} - N'''_{\text{pore}}(D_{\text{wick,i}})V_{\text{pore}}(\xi) \,, & \alpha_v \leq \alpha_v^{\text{wick,i,0}} \\ \alpha_v^{\text{wick,i,0}} + N'''_{\text{pore}}(D_{\text{wick,i}})V_{\text{pore}}(\xi) \,, & \alpha_v > \alpha_v^{\text{wick,i,0}} \end{cases} \tag{36}$$

where $V_{\text{pore}}(\xi)$ denotes the volume of a single pore depression, given the contact angle:

$$V_{\text{pore}}(\xi) = \frac{\pi R_{\text{pore}}^3}{3} (2+\xi) \sqrt{\frac{1-\xi}{(1+\xi)^3}}, \tag{37}$$

which, for example, corresponds to a perfect hemisphere if $\xi = 0$ and a flat surface if $\xi = 1$. Solving Equation (36) for ξ gives an following analytic expression for the sine of the contact angle as a function of void fraction:

$$\xi(\alpha_v) = \frac{1}{C_2} + \frac{C_2}{C_1 + 1} - 1, \tag{38a}$$

$$C_1(\alpha_v) = \left(\frac{3\left(\alpha_v - \alpha_v^{\text{wick,i,0}}\right)}{\pi R_{\text{pore}}^3 N_{\text{pore}}'''} \right)^2, \tag{38b}$$

$$C_2(\alpha_v) = \sqrt[3]{(C_1+1)^2 + \sqrt{C_1\left(1 + C_1\left(3 + C_1\left(3 + C_1\right)\right)\right)}}. \tag{38c}$$

Putting everything together, the capillary pressure difference can then be expressed by the following conditional relation:

$$\xi(\alpha_v) = \begin{cases} 1, & \alpha_v \leq \alpha_v^{\text{wick,i,}-} \\ \frac{1}{C_2} + \frac{C_2}{C_1+1} - 1, & \alpha_v^{\text{wick,i,}-} < \alpha_v < \alpha_v^{\text{wick,i,0}} \\ 1, & \alpha_v = \alpha_v^{\text{wick,i,0}} \\ \frac{1}{C_2} + \frac{C_2}{C_1+1} - 1, & \alpha_v^{\text{wick,i,0}} < \alpha_v < \alpha_v^{\text{wick,i,}+} \\ 0, & \alpha_v^{\text{wick,i,}+} \leq \alpha_v < \alpha_v^{\text{wick,o,}+} \\ 1, & \alpha_v \geq \alpha_v^{\text{wick,o,}+} \end{cases}. \tag{39}$$

Figure 4 shows an example of the contact angle dependence on void fraction.

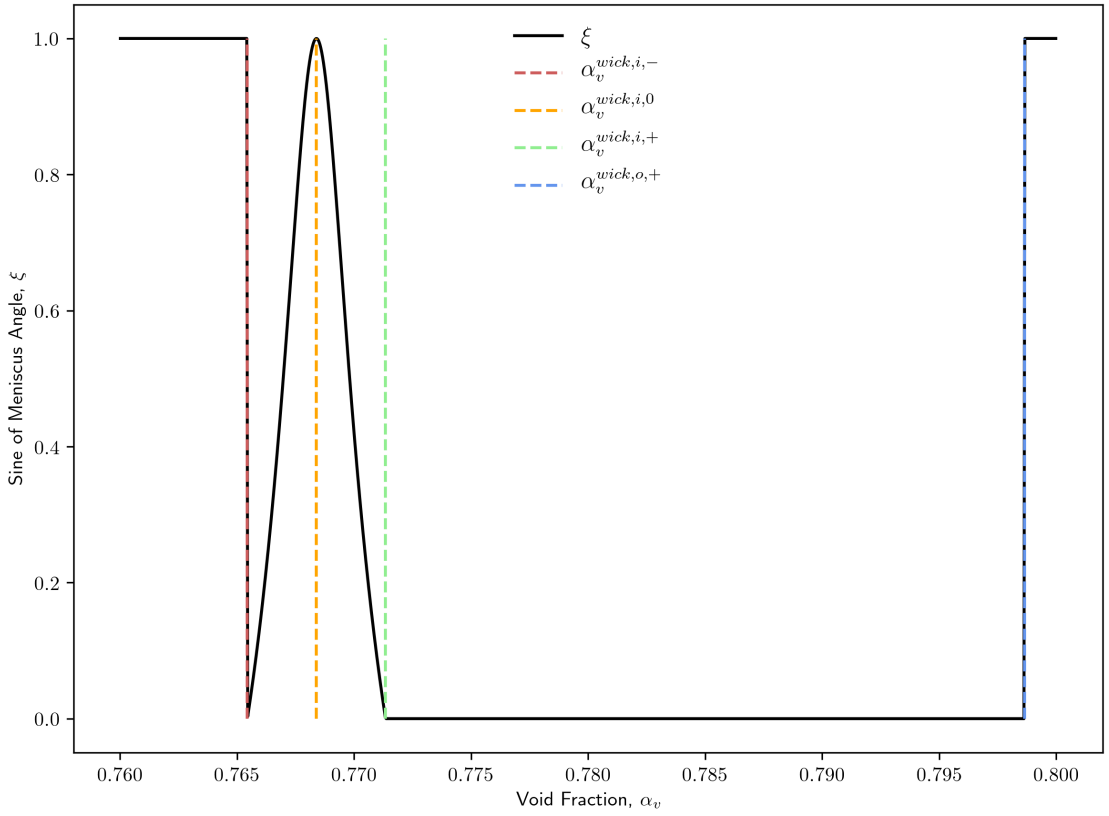

Figure 4: Contact angle vs. void fraction

3.2.2 Capillary Pressure

The capillary pressure difference between the phases is a function of the capillary radius; the sign depends on whether the interface is bulging outward or inward:

$$\Delta p^{\text{cap}}_{\ell\to v}(\alpha_v) = \begin{cases} 0\,, & \xi = 1 \\ -\frac{2\sigma}{R_{\text{cap}}(\xi)}\,, & \xi \neq 1\,, \alpha_v < \alpha_v^{\text{wick,i,0}} \\ \frac{2\sigma}{R_{\text{cap}}(\xi)}\,, & \xi \neq 1\,, \alpha_v > \alpha_v^{\text{wick,i,0}} \end{cases} . \tag{40}$$

Figure 5 shows an example of the capillary pressure dependence on void fraction.

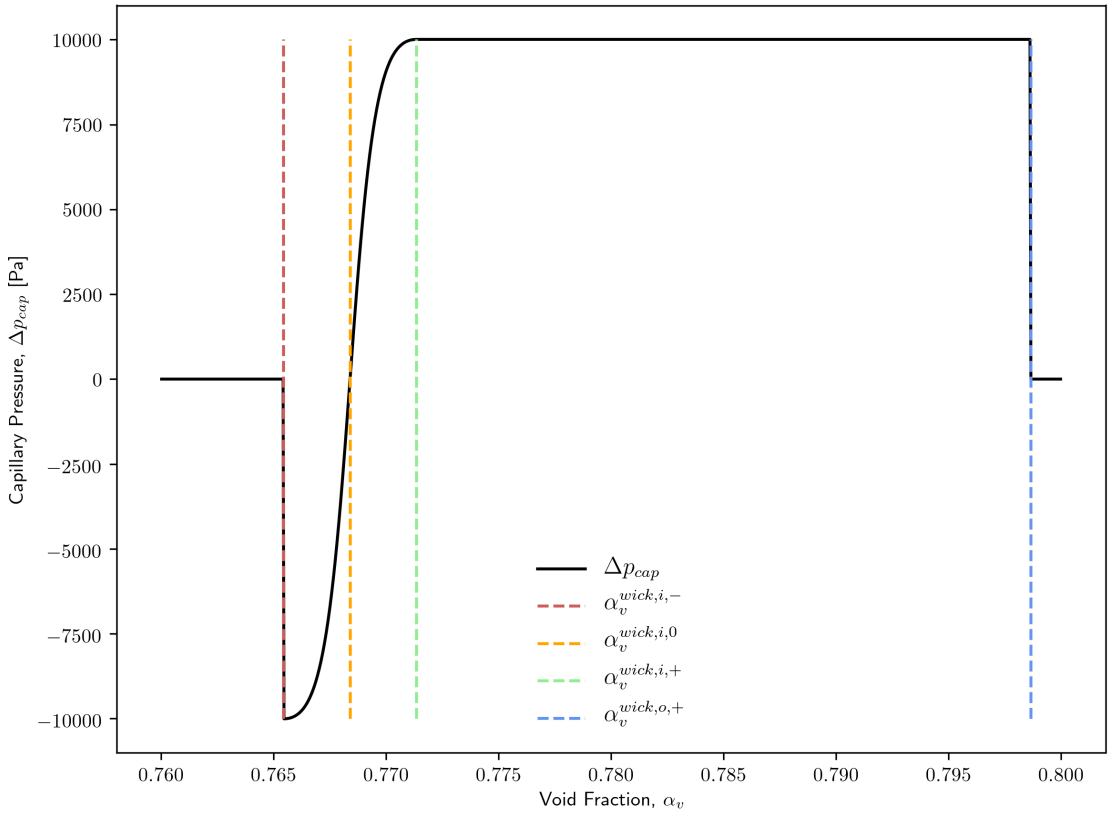

Figure 5: Capillary pressure vs. void fraction

3.2.3 Interfacial Area Density

For the case $\alpha_v \leq \alpha_v^{\text{wick,i,}-}$, the interfacial area density is

$$a_{\text{int}} = \frac{S_{\text{int}}}{V_{\text{flow}}} = \frac{P_{\text{int}} L_{\text{hp}}}{A_{\text{flow}} L_{\text{hp}}} = \frac{P_{\text{int}}}{A_{\text{flow}}} = \frac{\pi D_{\text{int}}}{A_{\text{flow}}} \,. \tag{41}$$

The correponding diameter of the vapor flow is found by equating the vapor flow area to the area of a circle:

$$\alpha_v A_{\text{flow}} = \frac{\pi D_{\text{int}}^2}{4} \,. \tag{42}$$

Then,

$$D_{\text{int}} = 2\sqrt{\frac{\alpha_v A_{\text{flow}}}{\pi}} \,. \tag{43}$$

For the case $\alpha_v^{\text{wick,i,}-} < \alpha_v \leq \alpha_v^{\text{wick,i,}+}$, the interfacial area density can be derived analytically as follows:

$$a_{\text{int}} = N'''_{\text{pore}}(D_{\text{wick,i}}) S_{\text{pore}} \,, \tag{44}$$

where the area of a single pore surface is

$$S_{\text{pore}}(\xi) = \frac{2\pi R_{\text{pore}}^2}{1+\xi} \,. \tag{45}$$

For the case $\alpha_v^{\text{wick,i,}+} < \alpha_v \leq \alpha_v^{\text{wick,0,}+}$,

$$a_{\text{int}} = N'''_{\text{pore}}(D) S_{\text{pore}}(0) = N'''_{\text{pore}}(D) 2\pi R_{\text{pore}}^2 \,. \tag{46}$$

The diameter D of the interface can be related to void fraction as follows:

$$\alpha_v = \alpha_v^{\text{wick,i,0}} + \frac{\epsilon\pi(D^2 - D_{\text{wick,i}}^2)}{4A_{\text{flow}}} + N'''_{\text{pore}}(D) V_{\text{pore,hemi}} \,. \tag{47}$$

Putting this in quadratic form and solving for the root that gives a positive diameter gives

$$D = \frac{-b + \sqrt{b^2 - 4ac}}{2a} \,. \tag{48a}$$

$$a = \frac{\epsilon\pi}{4} \,, \tag{48b}$$

$$b = \frac{\epsilon \pi V_{\text{pore,hemi}}}{A_{\text{pore}}}\,, \tag{48c}$$

$$c = (\alpha_v^{\text{wick,i,0}} - \alpha_v) A_{\text{flow}} - \frac{\epsilon \pi D_{\text{wick,i}}^2}{4}\,. \tag{48d}$$

For the case $\alpha_v > \alpha_v^{\text{wick,o,+}}$, the interfacial area density is

$$a_{\text{int}} = \frac{S_{\text{int}}}{V_{\text{flow}}} = \frac{P_{\text{int}} L_{\text{hp}}}{A_{\text{flow}} L_{\text{hp}}} = \frac{P_{\text{int}}}{A_{\text{flow}}} = \frac{\pi D_{\text{int}}}{A_{\text{flow}}}\,. \tag{49}$$

The correponding diameter of the vapor flow is

$$(1 - \alpha_v) A_{\text{flow}} = \frac{\pi}{4}(D_{\text{hp,i}}^2 - D_{\text{int}}^2)\,. \tag{50}$$

Then,

$$D_{\text{int}} = \sqrt{D_{\text{hp,i}}^2 - \frac{4(1-\alpha_v)A_{\text{flow}}}{\pi}}\,. \tag{51}$$

Putting everything together,

$$a_{\text{int}}(\alpha_v) = \begin{cases} \frac{2\pi}{A_{\text{flow}}} \sqrt{\frac{\alpha_v A_{\text{flow}}}{\pi}}\,, & \alpha_v \le \alpha_v^{\text{wick,i,-}} \\ \frac{2\pi R_{\text{pore}}^2 N_{\text{pore}}'''(D_{\text{wick,i}})}{1+\xi}\,, & \alpha_v^{\text{wick,i,-}} < \alpha_v \le \alpha_v^{\text{wick,i,+}} \\ 2\pi R_{\text{pore}}^2 N_{\text{pore}}'''(D)\,, & \alpha_v^{\text{wick,i,+}} < \alpha_v \le \alpha_v^{\text{wick,0,+}} \\ \frac{\pi}{A_{\text{flow}}} \sqrt{D_{\text{hp,i}}^2 - \frac{4(1-\alpha_v)A_{\text{flow}}}{\pi}}\,, & \alpha_v > \alpha_v^{\text{wick,o,+}} \end{cases}\,. \tag{52}$$

Figure 6 shows how the interfacial area density varies with void fraction.

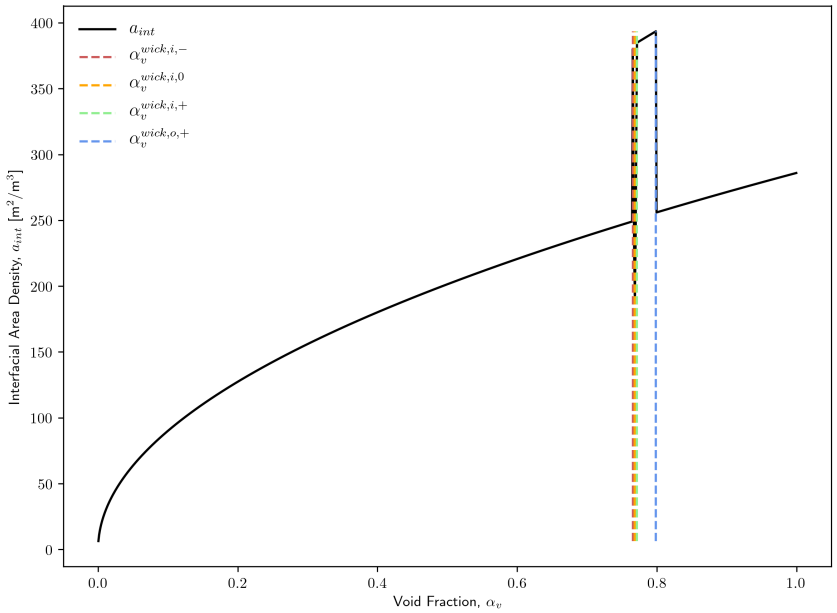

(a) All void fractions

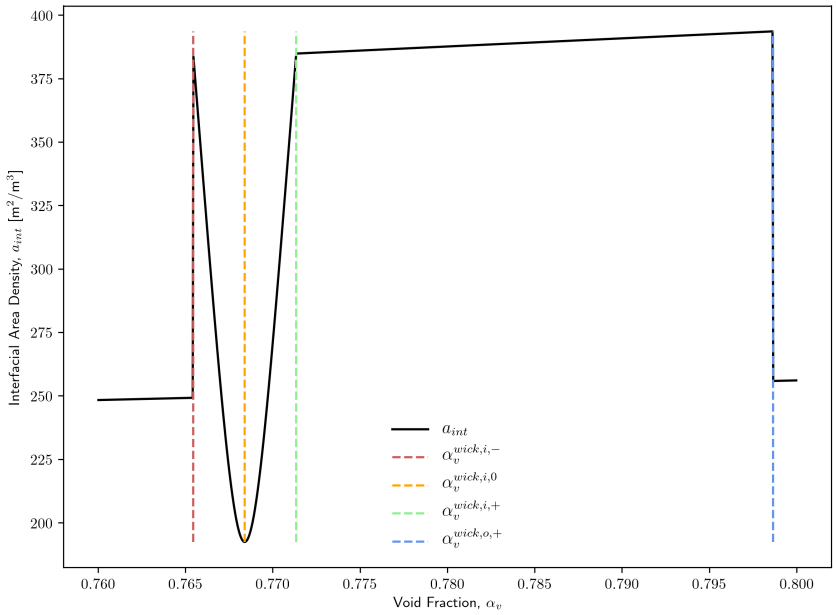

(b) Zoom view of wick region

Figure 6: Interfacial area density vs. void fraction

3.2.4 Wall Friction

The wall friction force acts opposite to the direction of flow. Using a *Darcy* friction factor $f_{\mathrm{D},k}$, the friction force density F_k^{wall} in Equations (14) and (17) is the following:

$$F_k^{\mathrm{wall}} = \frac{1}{2}\frac{f_{\mathrm{D},k}\rho_k \left|u_k\right| u_k}{D_{\mathrm{h},k}}\,, \tag{53}$$

where $D_{\mathrm{h},k}$ is the hydraulic diameter associated with phase k. For the vapor core, wall friction is due to the inner surface of the wick:

$$D_{\mathrm{h},v} = D_{\mathrm{wick,i}}\,, \tag{54}$$

whereas for the liquid channel, wall friction is assumed due to the inner wall of the heat pipe (a separate term is used to implement drag due to flow through the wick structure):

$$D_{\mathrm{h},\ell} = \frac{4(\epsilon A_{\mathrm{wick}} + A_{\mathrm{ann}})}{\pi D_{\mathrm{hp,i}}}\,. \tag{55}$$

The friction factors are determined by correlations that generally depend on the Reynolds number of the flow and the roughness of the surfaces. Currently, these are user-input constants.

3.2.5 Interfacial Heat and Mass Transfer

The interfacial mass flux $\Gamma_{\ell\to v}^{\mathrm{int}}$ is derived by summing the interfacial heat and mass transfer terms in the energy equations to give an energy balance statement for the interface:

$$\Gamma_{\ell\to v}^{\mathrm{int}} a_{\mathrm{int}} A \left(E_v^{\mathrm{int}} - E_\ell^{\mathrm{int}}\right) + q_\ell^{\mathrm{int}} a_{\mathrm{int}} A + q_v^{\mathrm{int}} a_{\mathrm{int}} A = 0\,. \tag{56}$$

Note that $E_v^{\mathrm{int}} - E_\ell^{\mathrm{int}} = h_v^{\mathrm{int}} - h_\ell^{\mathrm{int}} = h_{\ell v}(\bar{p}_{\mathrm{int}}, T_{\mathrm{int}})$, where $h_{\ell v}$ is the latent heat of vaporization. For phase k, the interfacial heat flux is

$$q_k^{\mathrm{int}} = \mathcal{H}_k^{\mathrm{int}}(T_{\mathrm{int}} - T_k)\,, \tag{57}$$

where the interfacial heat transfer coefficients $\mathcal{H}_k^{\mathrm{int}}$ are given by closure relations or user-defined constants.

Solving for the mass flux gives the following definition, which is independent of the definitions of the interfacial heat transfer coefficients:

$$\Gamma_{\ell\to v}^{\mathrm{int}} = \frac{\mathcal{H}_\ell^{\mathrm{int}}(T_\ell - T_{\mathrm{int}}) + \mathcal{H}_\ell^{\mathrm{int}}(T_v - T_{\mathrm{int}})}{h_v^{\mathrm{int}} - h_\ell^{\mathrm{int}}}\,. \tag{58}$$

Thus the interfacial mass flux is simply the net heat transferred to the interface divided by the latent heat.

3.3 Spatial Discretization

Sockeye uses the same spatial discretization as RELAP-7 [4], so only the differences need to be discussed. Sockeye adds a heat conduction term to the liquid phase, as shown in Equation (15). This term is approximated using a central difference:

$$\frac{\partial}{\partial x}\left(\alpha_\ell k_\ell \frac{\partial T_\ell}{\partial x} A\right)\bigg|_{i+1/2} \approx \alpha_{\ell,i+1/2} k_{\ell,i+1/2} \frac{T_{i+1} - T_i}{x_{i+1} - x_i} A_{i+1/2}\,, \tag{59}$$

where

$$\alpha_{\ell,i+1/2} \equiv \frac{1}{2}\left(\alpha_{\ell,i} + \alpha_{\ell,i+1}\right)\,, \tag{60}$$

$$k_{\ell,i+1/2} \equiv \frac{1}{2}\left(k_{\ell,i} + k_{\ell,i+1}\right)\,. \tag{61}$$

4 Startup and Shutdown Model

Because typical liquid-metal heat pipe working fluids are solid at room temperature, a melt phase must occur before normal operation of the heat pipe. Simulations that include startup and/or shutdown of a heat pipe thus must model the transition between the solid phase and the liquid and vapor phases. Two general approaches can be identified for the melting of the solid:

- Aggregate melting, and
- 3-phase modeling.

In the first approach, discussed in Section 4.1, the 2-phase (liquid and vapor) flow equations are not modified; they just remain inactive until the solid is considered fully melted. In the second approach, the 2-phase model is replaced by a 3-phase model, in which a given location may contain any number of the 3 phases. Currently, Sockeye is not capable of taking the 3-phase modeling approach, but this is intended for future capability.

4.1 Aggregate Melting Model

In this model, the 2-phase (liquid and vapor) flow equations are left unmodified but are not actually used until some appropriate fluid start condition is met. During this period, the sum effects of heat transfer on the heat pipe are applied to a single mass until this mass satisfies the fluid start condition, at which point the 2-phase flow simulation begins.

At a minimum the user must provide the following:

- m, total mass of the fluid/solid,
- T_0, initial, uniform temperature of the mass, and
- p_0, initial, uniform pressure of the mass.

The following initial value problem is solved to compute the specific enthalpy:

$$m\frac{\mathrm{d}h}{\mathrm{d}t} = \int_{\partial\Omega} q \,\mathrm{d}A\,, \qquad h(0) = h(p_0, T_0)\,, \tag{62}$$

where

- h is the specific enthalpy of the mass,
- $\partial\Omega$ is the boundary of the mass,
- q is the heat flux to the mass at a given spatial location, and
- $h(p, T)$ is the specific enthalpy of the mass (whatever phase it is in), as a function of pressure and temperature.

Physically, the heat flux integral depends on the distribution of the solid and the heat load on the heat pipe. Generally, the surface of the solid will partially be in contact with the heat pipe inner walls, with the rest either in contact with the wick or with a vacuum or low-pressure vapor. For a simple approximation, the solid can be approximated to be uniformly distributed along the heat pipe wall in the evaporator region only. Modeling the heat flux as

$$q = \mathrm{h}(T_{\text{wall}} - T)\,, \tag{63}$$

the heat flux integral can be expressed as follows:

$$\int_{\partial\Omega_s} q \,\mathrm{d}A = \int_{x_0}^{x_1} \mathrm{h}(T_{\text{wall}} - T) P_{\text{wall}} \,\mathrm{d}x\,, \tag{64}$$

where x_0 and x_1 are the x-limits of the 1-D heat pipe domain over which heat transfer can occur, such as the evaporator region alone. Alternatively, the integration can occur over the entire heat pipe length but with h set to zero outside of the evaporator. It is important not to perform heat transfer on the entire length because then the solid would effectively act as an infinitely conductive medium between the evaporator region and condenser region, thus avoiding the need of the working fluid to even be a fluid for effective operation of the heat pipe.

Now the start condition for fluid simulation needs to be discussed. If fluid simulation began at the melting point, then one would have an issue with evaluating vapor fluid properties since they do not exist at this temperature and pressure. Thus, without robust phase disappearance capability ($\alpha_v = 0$), it is necessary to avoid evaluation at this thermodynamic state. To ensure that no such evaluation occurs, the fluid simulation is started at or after the saturation state. The user provides an operating temperature T_{op}, at which the fluid simulation begins, giving the following fluid start condition:

$$T(h) \geq T_{\text{op}}\,. \tag{65}$$

At this point, the fluid is assumed to start at rest ($u_\ell = u_v = 0$) at some pressure p_0 and the corresponding saturation temperature $T_0 = T_{\text{sat}}(p_0)$. To determine this pressure and the initial void fraction $\alpha_{v,0}$, conservation of mass and energy equations are solved for the unknowns $\alpha_{v,0}$ and p_0:

$$m = \alpha_{v,0}\rho_v(p_0, T_{\text{sat}}(p_0))AL_{\text{hp}} + (1-\alpha_{v,0})\rho_\ell(p_0, T_{\text{sat}}(p_0))AL_{\text{hp}}\,, \tag{66}$$

$$\begin{aligned} mh = {} & \alpha_{v,0}\rho_v(p_0, T_{\text{sat}}(p_0))h_v(p_0, T_{\text{sat}}(p_0))AL_{\text{hp}} \\ & + (1-\alpha_{v,0})\rho_\ell(p_0, T_{\text{sat}}(p_0))h_\ell(p_0, T_{\text{sat}}(p_0))AL_{\text{hp}}\,. \end{aligned} \tag{67}$$

The initial conditions for the fluid simulation are then set as follows:

- $\alpha_v = \alpha_{v,0}$,
- $u_\ell = u_v = 0$,
- $p_\ell = p_v = p_0$, and
- $T_\ell = T_v = T_{\text{sat}}(p_0)$.

Alternatively, if it is deemed more important to start with a given volume fraction to ensure that the wick is exactly full:

$$\alpha_{v,0} = \frac{A_{\text{core}}}{A}\,, \tag{68}$$

then one needs to instead choose to not use the same total mass between the solid and fluid simulations but instead use fm, where f denotes the fraction of mass that is added/removed to achieve the given void fraction. Thus Equations (66) and (67) are modified as follows to solve for the unknowns f and p_0:

$$fm = \alpha_{v,0}\rho_v(p_0, T_{\text{sat}}(p_0))AL_{\text{hp}} + (1-\alpha_{v,0})\rho_\ell(p_0, T_{\text{sat}}(p_0))AL_{\text{hp}}\,, \tag{69}$$

$$\begin{aligned} fmh = {} & \alpha_{v,0}\rho_v(p_0, T_{\text{sat}}(p_0))h_v(p_0, T_{\text{sat}}(p_0))AL_{\text{hp}} \\ & + (1-\alpha_{v,0})\rho_\ell(p_0, T_{\text{sat}}(p_0))h_\ell(p_0, T_{\text{sat}}(p_0))AL_{\text{hp}}\,. \end{aligned} \tag{70}$$

For the heat flux defined by Equation (63), one needs to estimate the temperature T of the mass, given the specific enthalpy and pressure. An approximate equation of state for this is as follows:

$$T(p,h) = \begin{cases} T_v(p,h)\,, & h > h_{\text{sat},v}(p) \\ T_{\text{sat}}(p)\,, & h_{\text{sat},\ell}(p) < h \leq h_{\text{sat},v}(p) \\ \tilde{T}_\ell(p,h)\,, & h_{\text{melt},\ell}(p) < h \leq h_{\text{sat},\ell}(p) \\ T_{\text{melt}}(p)\,, & h_{\text{melt},s}(p) < h \leq h_{\text{melt},\ell}(p) \\ T_s(p,h)\,, & h \leq h_{\text{melt},s}(p) \end{cases}, \tag{71a}$$

$$h_{\text{sat},\ell}(p) \equiv h_\ell(p, T_{\text{sat}}(p))\,, \tag{71b}$$

$$h_{\text{melt},\ell}(p) \equiv h_\ell(p, T_{\text{melt}}(p))\,, \tag{71c}$$

$$h_{\text{melt},s}(p) \equiv h_{\text{melt},\ell}(p) - \Delta h_{\text{melt}}(p)\,, \tag{71d}$$

$$\tilde{T}_\ell(p,h) \equiv T_{\text{melt}}(p) + \frac{h - h_{\text{melt},\ell}(p)}{\tilde{c}_{p,\ell}(p)}\,, \tag{71e}$$

$$\tilde{c}_{p,\ell}(p) \equiv \frac{h_{\text{sat},\ell}(p) - h_{\text{melt},\ell}(p)}{T_{\text{sat}}(p) - T_{\text{melt}}(p)}\,, \tag{71f}$$

$$T_s(p,h) \equiv T_{\text{melt}}(p) + \frac{h - h_{\text{melt},s}(p)}{c_{p,s}(p)}\,. \tag{71g}$$

If one wants to compute the initial condition for h from p and T, then one needs to invert Equation (71). Here it is assumed that the user does not start in the middle of melting or saturation:

$$h(p,T) = \begin{cases} h_{\text{melt},\ell}(p) + \tilde{c}_{p,\ell}(p)(T - T_{\text{melt}}(p))\,, & T \geq T_{\text{melt}}(p) \\ h_{\text{melt},s}(p) + c_{p,s}(p)(T - T_{\text{melt}}(p))\,, & T < T_{\text{melt}}(p) \end{cases}. \tag{72}$$

5 Multiphysics Coupling

Sockeye can be coupled to other physics applications, typically via various heat transfer boundary conditions.

The most common form of coupling with Sockeye will occur via convective heat transfer computed using temperatures from Sockeye and another application. The wall temperature along the 1-D flow domain, or the outer temperature in a 2-D solid domain, can be transferred from another application, from a 1-D, 2-D, or 3-D domain, allowing convective heat fluxes to be computed:

$$q = \mathrm{h}(T_{\text{wall}} - T)\,. \tag{73}$$

Future couplings could include the thermal expansion of the heat pipe, axially or radially. This would lengthen the flow domain or change the flow area, respectively.

References

[1] D. R. Gaston, C. J. Permann, J. W. Peterson, A. E. Slaughter, D. Andrš, Y. Wang, M. P. Short, D. M. Perez, M. R. Tonks, J. Ortensi, L. Zou, and R. C. Martineau, "Physics-based multiscale coupling for full core nuclear reactor simulation," *Annals of Nuclear Energy*, vol. 84, pp. 45–54, 2015.

[2] A. Faghri, *Heat Pipe Science and Technology*. Global Digital Press, second ed., 2016.

[3] D. A. Reay, P. A. Kew, and R. J. McGlen, *Heat Pipes: Theory, Design and Applications*. Elsevier Ltd., sixth ed., 2014.

[4] R. A. Berry, J. W. Peterson, H. Zhang, R. C. Martineau, H. Zhao, L. Zou, D. Andrš, and J. E. Hansel, "RELAP-7 theory manual," Tech. Rep. INL/EXT-14-31366, Idaho National Laboratory, March 2018. Revision 3.

[5] R. A. Berry, R. Saurel, and O. LeMetayer, "The discrete equation method (DEM) for fully compressible, two-phase flows in ducts of spatially varying cross-section," *Nuclear Engineering and Design*, vol. 240, pp. 3797–3818, 2010.

[6] A. Chinnayya, E. Daniel, and R. Saurel, "Modelling detonation waves in heterogeneous energetic materials," *Journal of Computational Physics*, vol. 196, pp. 490–538, 2004.


INL
Idaho National Laboratory